Available online at www.sciencedirect.com

ScienceDirect

Procedia Structural Integrity 8 (2018) 354–367

Structural Integrity Procedia

www.elsevier.com/locate/procedia

AIAS 2017 International Conference on Stress Analysis, AIAS 2017, 6-9 September 2017, Pisa, Italy

Quantitative analysis of thermographic data through different algorithms

E. D'Accardi; D. Palumbo; R. Tamborrino; U. Galietti

Politecnico di Bari - Dipartimento di Meccanica, Matematica e Management, Viale Japigia 182, 70126 Bari, e-mail: ester.daccardi@poliba.it, davide.palumbo@poliba.it, rosanna.tamborrino@poliba.it, umberto.galietti@poliba.it.

Abstract

Pulsed thermography is commonly used as non-destructive technique for evaluating defects within materials and components. However, raw thermal imaging data are usually not suitable for quantitative evaluation of defects. It was necessary to process the raw thermal data acquired to obtain a series of satisfactory results for a correct and quantitative material evaluation. In the last years, many data processing algorithms have been developed and each of them provide enhanced detection and sizing of flaws.
In this work, starting from the same brief pulsed thermographic test carried out on an aluminium specimen with twenty flat bottom holes of known nominal size, different algorithms have been compared. The algorithms used have been: Pulsed Phase Thermography (PPT), Slope, Correlation Coefficient (R^2), Thermal Signal Reconstruction (TSR), Principal Component Analysis (PCT). By analysing the results obtained using different approaches, it was possible to focus on the advantages, disadvantages and sensitivity of the various thermographic algorithms implemented.

Keywords: Pulsed thermography; Algorithm; PPT; PCT; TSR; R^2; Slope.

1. Introduction.

In the aeronautics field, during manufacturing process, random porosity or several defects may appear in mechanical structures. These undesirable defects affect the structure and its mechanical properties. In this regard, it is very important to check the integrity of the components to reveal these defects.

Several non-destructive techniques can be used to detect such defects.

2452-3216
10.1016/j.prostr.2017.12.036

In the last period, the thermographic technique is becoming more and more established for detecting the integrity of a structure and can be considered one of the most innovative, fast and non-contact investigation techniques to detect defects and anomalies in mechanical materials, Maldague X. P. V. (2001), Palumbo D. et all (2016), Tamborrino R. et all (2016), Palumbo D. et all (2016), Palumbo D. et all (2017), Palumbo D. et all (2017), Galietti U. et all (2012), Galietti U. et all (2012)

However, in literature, it lacks a quantitative analysis of the acquired thermal data with the aim to determine the dimension, depth and shape of defects. Raw thermal imaging thermographic data are usually not suitable for a direct quantitative material evaluation and the development of data processing methods to detect defects features as well as to determine the defect sizes and material parameters is essential for the correct application of the thermographic technique, Sun J. (2013), Balageas D.L. (2012), Junyan L. (2016).

In this work, the attention has been focused on the Pulsed Thermography (PT) technique applied on an aluminium specimen with flat bottom holes to simulate the presence defects. PT employs a short thermal stimulation to produce a thermal perturbation within the material. The presence of a defect can be revealed by monitoring the surface temperature decay of the specimen. In fact, the defect appears as an area of different temperature with respect to a surrounding sound area and it produces an abnormal behaviour of the temperature decay curve, Maldague X. P. V. (2001). It should also be pointed out that aluminium is a particular material, because of its thermal diffusivity, therefore it is difficult to apply thermographic techniques on it.

Several algorithms have been implemented to elaborate raw thermal data and to characterize the defects, such as Pulsed Phase Thermography (PPT), Principal Component Thermography (PCT), Thermal Signal Reconstruction (TSR), Slope, Correlation coefficient (R^2), in order to compare the same. The algorithms were compared in terms of the number of detected defects, the contrast between the defect and the sound area and data processing speed, to establish which applied algorithms returns the best quantitative results, Sun J. (2013), Hidalgo-Gato R. et all (2013), Hidalgo-Gato R. et all (2013), Bendada A. et all (2007), Ibarra-Castanedo C. et all (2005), Shepard S. M. (2001).

In this work, it wants to propose a semi-automatic approach to analyse the thermographic maps obtained with the various proposed algorithms to derive quantitative information from the acquired data in order to characterize the researched defects. In particular, a procedure has been developed in order to determine whether a defect is detected or not by a calculator.

2. Pulsed infrared thermography and algorithms used to elaborate the acquired data.

2.1. Pulsed infrared thermography

The pulsed thermography consists of a short heating of the sample, followed by recording temperature decay curve Maldague X. P. V. (2001).

Immediately after the heat pulse deposition stops, it is possible to consider that the cooling behavior of tested sample is the same of a semi-infinite homogeneous sample characterized by an effusivity in the *z* direction e_z. Then the surface temperature time evolution follows law:

$$\Delta T_{xy}(t) = \frac{Q_{xy}}{e_z\sqrt{\pi t}} \tag{1}$$

Where ΔT_{xy} is the increasing of temperature (in *x* and *y* directions), Q_{xy} is the energy absorbed by the surface and *t* is the time.

The presence of a defect, because of the reduction of the diffusivity of the material near it, influences the surface temperature evolution, so that in the defected area the temperature is higher than in the sound area. Besides deeper defects are observed after a longer time and with a reduced thermal contrast.

The evolution of the thermal contrast on the defect and the equations resulting from the thermal wave theory allow to characterize the defect in terms of depth and diameter. The definition of the thermal contrast is:

$$C = \frac{T_{def}(t) - T_{def}(t_0)}{T_{sound}(t) - T_{sound}(t_0)} \tag{2}$$

where T is the temperature signal, t is the variable time, while the subscripts def and sound refer to the defect and sound area, respectively; the time t_0 is the time at which the cooling starts. In this work, a quantitative data analysis has been performed by referring to the normalized contrast C_n of tested parameters, such as the phase, the principal components, the slope and the correlation coefficient:

$$C_n = \frac{P_{def} - P_{sound}}{\sigma} \tag{3}$$

where P is the chosen parameter and σ is the standard deviation. All the relations have been normalized respect to σ to consider the noise influence and to compare the used algorithms.

2.2. Pulsed Phase thermography (PPT)

Pulsed phase thermography (PPT), Ibarra-Castanedo C. (2005), Maldague X. et all (1996), is a technique that transforms data in time domain into the frequency domain using Fast Fourier Transform (FFT). This algorithm combines the techniques of lock-in thermography and pulsed thermography, analyzing through the phase and amplitude parameters, the specimen cooling transition.

The extraction of various frequencies, to each of them corresponds a phase and amplitude maps, is done by using the FFT of the thermal signal for each pixel. This transformation is performed as:

$$\mathrm{F_n} = \Delta \mathrm{t} \sum_{\mathrm{k}=0}^{\mathrm{N-1}} \mathrm{T(k\Delta t)} \exp^{((\mathrm{-i2\pi nk/N}))} = \mathrm{Re_n} + \mathrm{Im_n} \tag{4}$$

where *Re* and *Im* are respectively the real part and imaginary part of the transformed and the subscript n is the increasing frequency. The maps are finally obtained using the following relation:

$$A_n = \sqrt{\mathrm{Re}_n^2 + \mathrm{Im}_n^2}\,(amplitude) \qquad \varphi_n = \tan^{-1}\frac{\mathrm{Im}_n}{\mathrm{Re}_n}\,(phase) \tag{5}$$

In general, N thermograms generate $N/2+1$ phase maps, associated with frequencies ranging from 0 to $N/2{*}\Delta f$, with $\Delta f = 1/t_{oss}$ (t_{oss} = observation time of heat phenomenon).

2.3. Principal component thermography (PCT)

As well as PPT, the Principal Component Thermography (PCT), Rajic N. (2002), Parvataneni R. (2009), transforms the raw thermography data using orthogonal base functions-the principal component. The Principal Component

Analysis (PCA) is a linear projection technique for converting a matrix A of dimension $m \times q$ to a matrix B of lower dimension $p \times q$ (with $p<m$) by projecting A onto a new set of principal axes. Matrix A is decomposed by singular value decomposition as:

$$A = USV^T \tag{6}$$

where U is an mxn column-orthogonal matrix, S is an nxn diagonal matrix and V is an nxn column-and row-orthogonal matrix. The uncorrelated variables are linear combinations of the original variables, and, in particular, the first component contain the data with higher variance, while the consecutive components are with decreasing variances, so they are the symbol of noise. Therefore, only a few components, in particular the second principal component, need to be examined in the thermography data analysis to underline the presence of a defect.

2.4. Thermographic signal reconstruction (TSR)

Thermographic signal reconstruction (TSR), Balageas D.L. et all (2013), Benitez H. et all (2006), Balageas D.L. et all (2010), assumes that temperature profiles for non-defective pixels should follow the decay curve given by the 1D solution of the Dirac equation, Eq.(1), which may be rewritten in the logarithmic polynomial form as:

$$\ln(\Delta T) = a_0 + a_1 \times \ln(t) + a_2 \times [\ln(t)]^2 + a_3 \times [\ln(t)]^3 + \ldots + a_n [\ln(t)]^n \tag{7}$$

where ΔT is the increasing of temperature and t is the time. Typically, n is set to 4 or 5 to assure a good correspondence between acquired data and fitted values while reducing the noise content in the signal. Then, the entire raw thermogram sequence is reduced to $n+1$ coefficient images (one per polynomial coefficient) from which synthetic thermograms can be reconstructed. Furthermore, the derivation being achieved directly on the polynomial give the 1st and 2nd logarithmic derivatives of the thermogram, then with a limited increase of the temporal noise. The first time-derivative indicates the rate of cooling while the second time-derivative refers to the rate of change in the rate of cooling. Therefore, time derivatives are more sensitive to temperature changes than raw thermal images. There are no purpose using derivatives of higher order; since, besides the lack of a physical interpretation, no further improvement in defect contrast is obtained.

2.5. Slope and correlation coefficient R^2

If it shows the trend of surface temperature change over time in a double logarithmic scale, the Eq.(1) becomes:

$$\ln(\Delta T) = \ln\left(\frac{Q}{e}\right) - \frac{1}{2}\ln(\pi t) \tag{8}$$

The trend is shown in the Fig.1, where it is possible to observe that an area free of defects (1), the temperature decay has slope of (-1/2) in the central part.

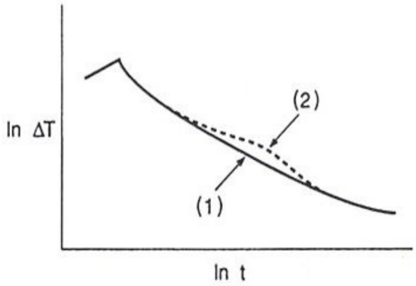

Figure 1. Trend of cooling curve in a double logarithmic scale.

If there is a defect in the depth (sub-surface) (2), the decay of the temperature variation is "deviate" from the homogeneous condition without defects and, in general, the slope is different to (-1/2).

In the presence of a defect, it is possible to notice a deviation of the cooling curve from a linear trend in a double logarithmic diagram, such as shown in Fig.1. A measure of this deviation is the square correlation coefficient R^2, Palumbo D. et all (2016).

In the work Palumbo D. et all (2016), the algorithms of the slope and the R^2 have been proposed for the first time to find defects within a composite sample, restoring competitive and comparable results with amplitude and phase maps typically used to analyze thermal data.

3. Material and methods.

An aluminum sample, with 20 flat bottom holes of different diameter and depth, has been tested-Fig.2. The different sizes of simulated defects are indicated in Tab.1.

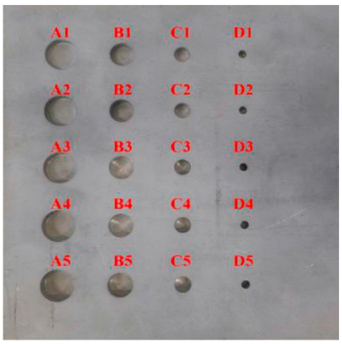

Figure 2. Aluminium sample.

Table 1: Sizes of flat bottom holes (aluminium sample in Fig.2).

NUMERATION OF FLAT BOTTOM HOLES (FIG.2)	DIAMETER	DEPTH
A1 A2 A3 A4 A5	A 16mm	A1 1mm A2 2mm A3 3mm A4 4mm A5 5mm
B1 B2 B3 B4 B5	B 12mm	B1 1mm B2 2mm B3 3mm B4 4mm B5 5mm
C1 C2 C3 C4 C5	C 8mm	C1 1mm C2 2mm C3 3mm C4 4mm C 5mm
D1 D2 D3 D4 D5	D 4mm	D1 1mm D2 2mm D3 3mm D4 4mm D5 5mm

A Pulsed Thermography test was performed using the IR camera FLIR X6540 SC with thermal sensitivity (NETD) < 25 mK and based on a cooled detector with 640×512 pixels. The set-up used is shown in Figure 3. In particular, two flash laps with an energy of 3000 J were positioned very close to the specimen (10 mm) and at the same side of the IR camera. This latter was placed at about 1 m from the specimen in order to obtain a geometrical resolution of 0.25 mm/pixel.

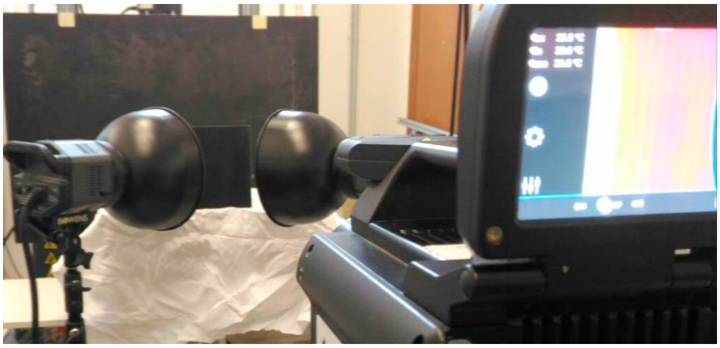

Figure 3. Set-up of test.

The thermal sequence was acquired with a sample rate of 200Hz, with an observation time of 5 seconds.

3.1. Analysis procedure of acquired data

The raw thermal data, provide only qualitative information in terms of signal variation between the sound and the defected area which need to be further elaborated.

Several algorithms, involving thermal and physical parameters of acquired data, have been developed to achieve the aims exposed in previous sections.

For all implemented algorithms, it has been chosen to analyse 256 frames of the decay curve corresponding to 1.28 s because, in this time interval, the thermal phenomenon can be considered terminated and because a FFT analysis requires a number of data equal to a power of two.

Then, the various algorithms have been applied by using different engineering software. In particular, the slope and the R^2 have been implemented on software IRTA®, while PPT, TSR and PCT have been developed with MATLAB®.

The application of these algorithms has required a further elaboration of acquired data to obtain better results. In particular, it has been necessary to normalize the local temperature rises recorded by infrared camera at any time by dividing them by those obtained at the same places at time t' sufficiently near of the pulse occurrence:

$$\Delta\overline{T}_{xy}(t) = \frac{\Delta T_{xy}(t)}{\Delta T_{xy}(t')} \tag{9}$$

This pixel-wise operation gives to each pixel, at time t', the value equal to 1 to the normalized temperature rise. Also, an advantage of this operation is to reduce the effects of non-perfect illumination and the variability of the optical properties of the surface, such as absorptivity and infrared emissivity.

For applying the PCT analysis, it has been necessary to subtract from the array of data the average of the same and to normalize respect to standard deviation, as indicated in the literature, Rajic N. (2002).

All algorithms have returned several types of thermographic maps, Fig.5; a gaussian filter has been applied, in all cases, on each thermographic map, in order to decrease the noise. It moved then to a quantitative analysis of the data from these maps to characterize defects on the analyzed component.

To characterize every flaw, it has been necessary to identify a sound zone to be taken as a reference. A common problem to all implemented methods is the definition of the sound zone. The goal of this work is, in fact, to identify and characterize the defects on the analysed component.

In literature, there is not a specific procedure to identify this zone unequivocally. For a pulsed thermographic test, several ways have been tested to define the sound reference: from a priori knowledge a part of an image is taken as the sound reference; a test sample is identical to the one analysed and within defects; in the single pixel analysis, the soundness is determined locally, for each pixel, considering the thermogram evolution at any time; with the method of the "contrast full-width at half-maximum", Giorleo G. et all (2002), Balageas D.L. et all (2017).

In this work, it has been chosen to use the "contrast full-width at half-maximum" method to locate the sound zone for each defect. However, this method is unattainable, because it is dependent on the nature of the physical and thermographic parameters that are being analysed, and, hence, from the sign change between the defect and the sound zone (Fig.4). This dependence from the sign makes non-automatic the procedure, and then make it rather slow if there are many thermographic maps to analyse (as in the case of this work) or if there are many defects in the tested specimens.

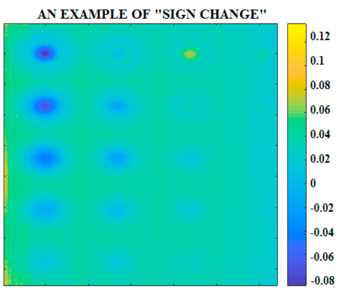

Figure 4. An example of "sign change": SECOND DERIVATIVE TSR, frame 40.

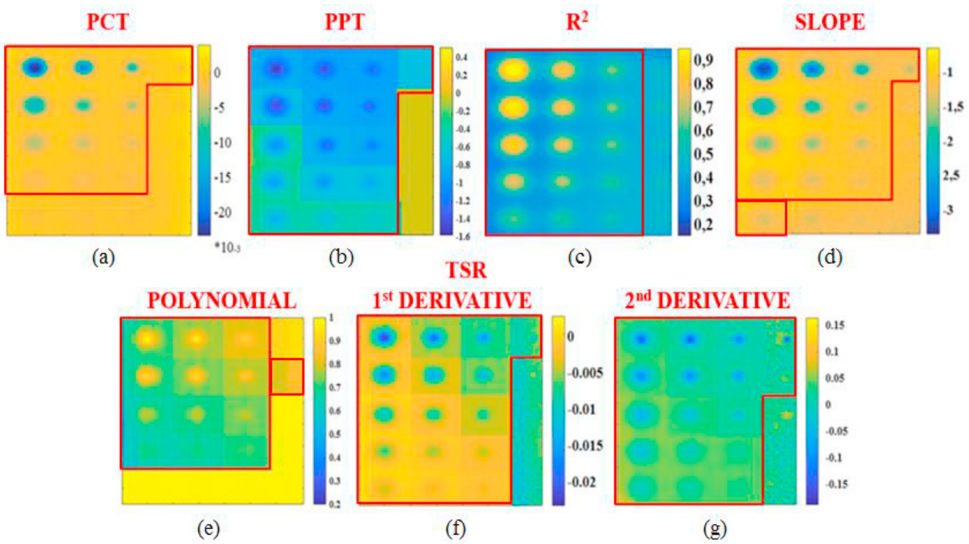

Figure 5. An example of obtained map for each applicated algorithm: (a) PCT; (b) PPT; (c) R^2; (d) Slope; (e) Fifth degree Polynomial TSR; (f) 1st derivative polynomial TSR; (g) 2nd derivative polynomial TSR.

Then, it has been used a new method to detect the sound and defect zone by analysing the trend of the standard deviation (std) of the acquired data. This new method, which for brevity will be indicated by the acronym "std method", is described below in detail and applied to the specific case study for each obtained map and for each applicated algorithm.

Several maps, similar to those reported in Fig.5, have been obtained. For brevity, each of these maps is explained in detail in the section of results.

For each defect, it has been chosen an area so as to consider the sound and the defect zone and to have the same number of pixels. In this way, a matrix has been obtained for each defect and so it has been calculated the trend of the standard deviation for row and for column, getting results similar to the following (example).

As you can see from Fig.6 and as might be expected, the trend of standard deviation shows a peak where the defect is present.

It has been chosen a threshold of 0.5 on the trend of standard deviation (which is the same in all algorithms) to discriminate the sound area from the defect area, Fig.6. In particular, to define this threshold, a delta has been calculated on the trend of standard deviation with reference to 98°percentil and 2°percentil; as highlighted in Fig.6, the sound area is that under the 0.5 threshold, while for the defect, after locating the peak of this trend, it has been chosen the pixels with value greater than the 98% of the peak value.

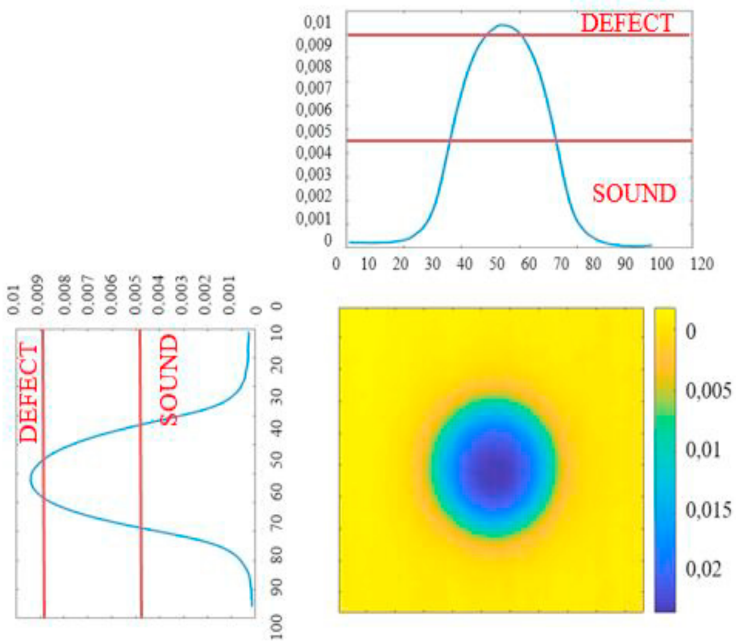

Figure 6. An example of the calculation procedure: the trend of standard deviation (first defect of PC2 map, diameter 16mm-depth 1mm)

This logic, used to detect the presence of the defect, has been maintained for each algorithm. To make automatic the research of the defects, the same threshold value has been mantained. In particular, the value of 0.5 referred to the standard deviation has been chosen for avoiding the overlapping of the defect zones which occurred in the maps extracted by using PPT algorithm. In these maps, because of the mutual influence among defects, another threshold value would have led to few pixel for evaluating the sound zones. However, as shown in Fig.7, for some algorithms, this choise has not been advantageous, because, when evaluating the sound area, there is also a presence of some defective pixels. So the normalized contrast is lower and the obtained result is more conservative.

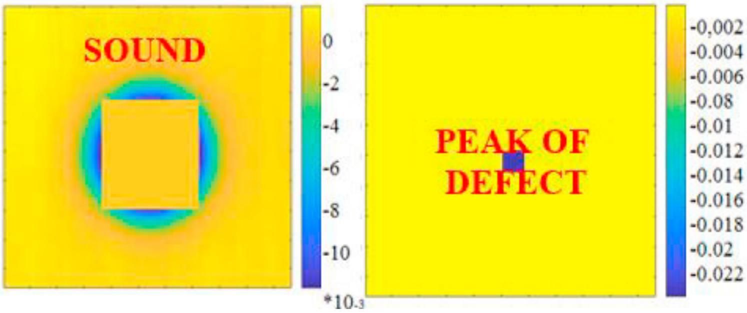

Figure 7. An example of sound and defect area, first defect of PC2 map (diameter 16mm, depth 1mm).

Then, the normalized contrast from Eq.(4), for each defect and for each physical and thermographic parameter has been calculated. The results obtained using the developed "standard deviation" method are in agreement with those obtained using "maximum semi-contrast" method, as it is shown in the following plot selected as example.

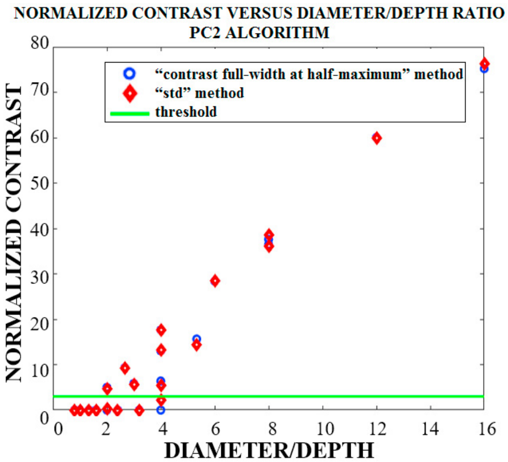

Figure 8. An example of the confront between "standard deviation" method and "maximum semi-contrast" method, normalized contrast on the PC2 map.

The plot in Fig.8 shows the trend of the normalized contrast versus the depth-diameter ratio for each defect. Very similar graphs have been obtained from the other developed algorithms.

For brevity, the results will be reported organized by algorithm and it will be shown the thermographic maps and the normalized contrast graphs obtained using the "standard deviation" method.

To determine if a defect can be distinguished in a thermographic map, a normalized contrast threshold was chosen as the value 3 (Fig.8):

$$C_n = \frac{P_{def} - P_{sound}}{\sigma} > 3 \tag{10}$$

The standard deviation has been evaluated with reference to the areas indicated in red in Fig.9.

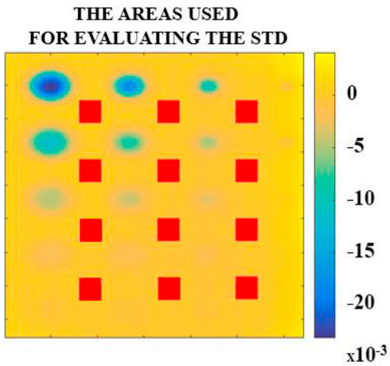

Figure 9. The areas used for evaluating the standard deviation (PCT2 map).

4. Results.

4.1. Principal Component Thermography (PCT) results

By applying the SVD (Singular Value Decomposition) algorithm, it has been possible to derive from the thermographic sequence the maps of the principal components (PCT's). The map of the second principal component (PCT2) is reported in Fig.5. Qualitatively, it is possible to distinguish 13/20 defects.

From the graph of normalized contrast versus the diameter-depth ratio (Fig.14), considering eq. 10, even the defect of 4mm diameter and 1mm depth cannot be distinguished by the algorithm. Quantitatively, then, 12/20 defects are detected. For brevity, the graphs of the normalized contrast are reported in the paragraph of the finally comparisons.

4.2. Pulsed Phase Thermography(PPT) results

By applying the FFT analysis on the thermographic sequence, a phase map has been obtained for each extracted frequency. For each defect, the trend of phase as a function of the frequency has been analyzed. In particular, the difference of this trend between the defect and the relative sound area shows a peak at the frequency which depends from the depth and the size of the defect. At this frequency, the contrast between the defect and the sound area is maximum. In Fig.10, an example of this trend is reported; the defect and the relative sound zone, to calculate these trends, have been identified with the "std method".

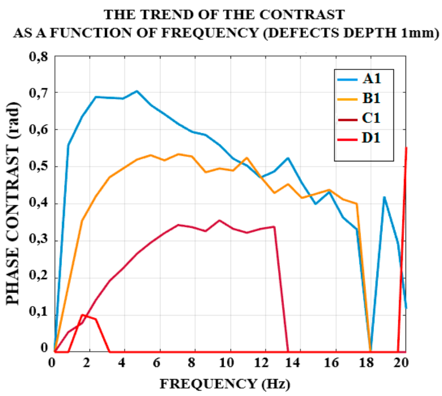

Figure 10. The trend of the contrast as a function of the frequency: defects at 1mm depth.

Then, the algorithm for the computing of the normalized contrast has been applied (Fig.14).

The results of individual maps related to the several frequencies have been compacted into a single map, choosing to show, for each defect, its maximum contrast (Fig.5). The calculator can distinguish 16/20 defects (Fig.14).

4.3. Signal Reconstruction Thermography (TSR) results

The thermographic sequence data have been analyzed with the TSR algorithm, choosing a polynomial of the fifth degree in double log-scale. The trends of the first and second derivative of this polynomial have been also analyzed. As the PPT case, an example of the obtained trends with reference to the defects at 1mm depth are shown in Fig.11.

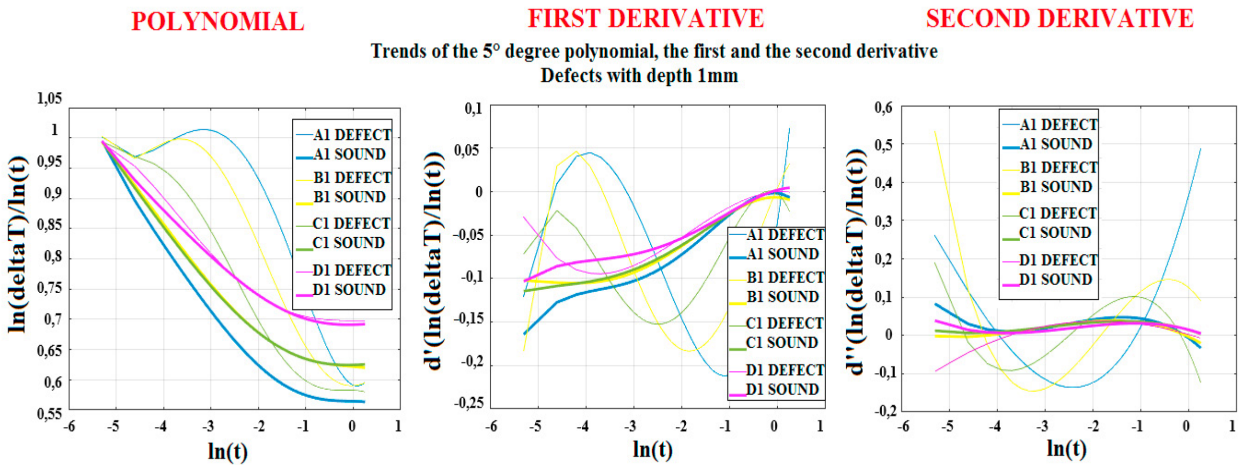

Figure 11. Trends of fifth degree polynomial, First Derivative Polynomial, Second Derivative Polynomial: comparison between sound and defective zones at 1mm of depth.

As shown in the graphs of Fig.11, in correspondence of a defect, there is a change of the polynomial trends. The differences between the sound and the defect area trends have been calculated, finding a maximum contrast value to a time that changes according to the size and the depth of the defect, Fig.12.

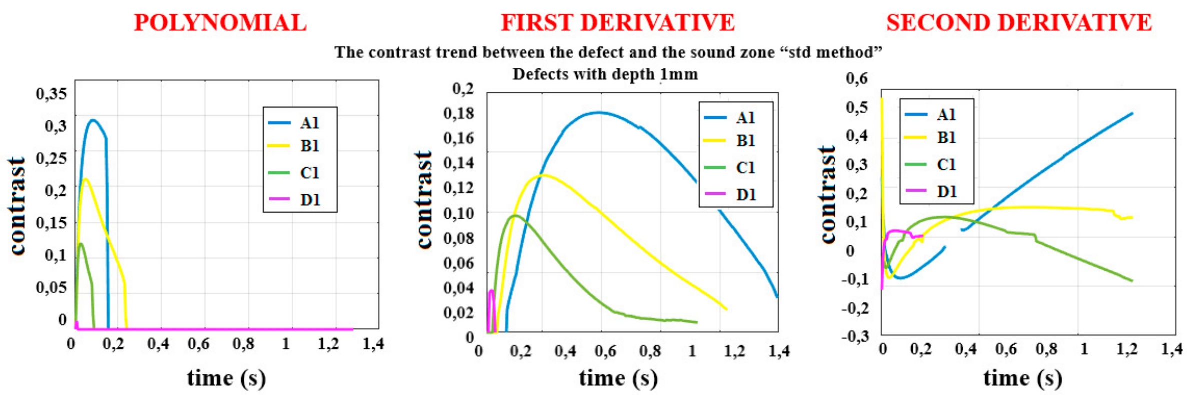

Figure 12. The contrast trend between the defect and the sound area, TSR algorithm (polynomial, first derivative, second derivative).

Once again, the map relating to the maximum contrast for each defect is shown in Fig.5. The results for the maximum contrast in terms of the first and the second derivative are certainly better than those of the simple polynomial: the maps are less noisy and a greater number of defects can be distinguished. In particular, in the second derivative polynomial case, the calculator can evaluate the presence of 17/20 defects.

The result of 17/20 defects, for the second derivative polynomial, is kept also analyzing the trend of the normalized contrast (Fig.14).

4.4. Slope and R^2 results

Using the software IRTA, the slope and R^2 algorithms have been applied to the thermographic sequence, in few minutes. This analysis allows to obtain a single map for each algorithm (Fig.5), on which the algorithm for the calculation of the normalized contrast has been applied. By analyzing these maps, it is known as the choice of keeping the same number of frames for all algorithms, has negatively affected the results obtained. In particular, the R^2 maps shows no sensitivity for the defects of 4 mm diameter.

The graphs of the normalized contrast (Fig.14) show the same results: the maps result very noisy, so several defects can't be detected.

5. Comparison of algorithms.

The results obtained for each algorithm have been compared in order to show the differences among the several algorithms implemented. The several algorithms have been compared in terms of:

- number of detected defects (columns in blue in Fig.13);
- number of detected defects with a specific depth (Fig.13a);
- number of detected defects with a specific diameter (Fig.13b);
- maximum normalized contrast (Fig.14).

The TSR algorithm, in particular, the second derivative of the polynomial, seems to return the best results: 17/20 defects have been detected at the calculator, with an elevate normalized contrast. The PPT algorithm shows a good sensitivity to detect the analyzed defects, with a number of 16/20 defects detected. However, the normalized contrast results obtained using PPT algorithm are much lower than the obtained TSR results. The PCT algorithm returns good results in terms of maximum normalized contrast, however doesn't show a great sensitivity in detecting both small and deep defects, for a total of 12/20 detectable defects. The algorithms of the R^2 and the slope do not show great results, in particular it seems that the R^2 is more influenced by the size of the defect (0/5 defects of 4mm diameter-Fig.13b) instead of the depth (2/4 defects of 5mm depth-Fig.13a), while for the slope algorithm the opposite occurs. These last algorithms show also fairly low contrast (Fig.14).

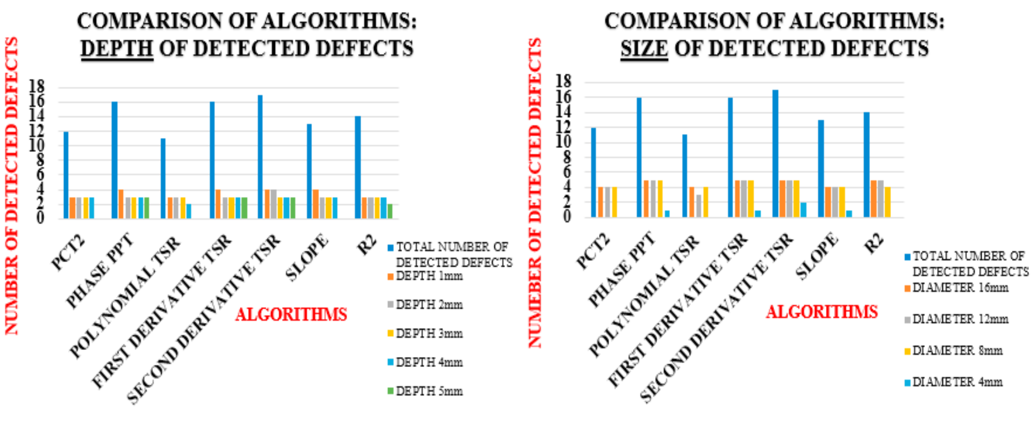

Figure 13. Comparison among the several algorithms in terms of depth (a) and size (b) of detected defects.

However, the speed of all these algorithms is quite important. In particular, the TSR algorithm takes a long time of analysis because it is obtained a map for each frame and because it is required a careful analysis of first and second derivative maps. An analysis of PPT type involves the same problems. The R^2 and the slope algorithms are, instead, much faster and they must be optimized in terms of frames to be analyzed.

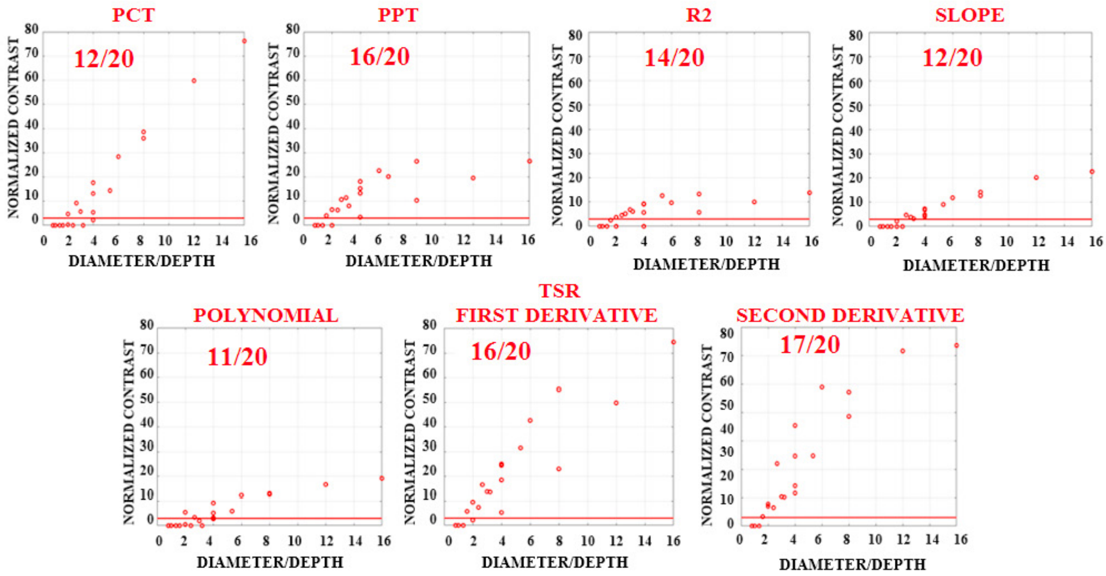

Figure 14. Comparison among the several algorithms in terms of maximum normalized contrast.

6. Conclusions.

A spaceman in aluminium with twenty imposed defects was analysed, in order to obtain a semiautomatic procedure to characterize the defects. Five different algorithms were compared highlighting their strength and weaknesses in terms of capacity in detection defects. A semiautomatic procedure was elaborated to evaluate quantitatively the bottom flaws in terms of contrast of various analysed parameters in order to determine whether a defect is detectable directly or not by a calculator. It seems that the TSR algorithm returns better results: analysing the trend of contrast from the map of the second derivative, it can detect 17/20 defects with a high contrast. However, the analysis of maps relating to this algorithm has taken quite longer time. Besides, it will need to optimize the processing parameters, such as the number of analysed frames, for R^2 and slope algorithms in order to achieve better results in less time.

References

Maldague X. P. V. (2001). Theory and practice of infrared technology of non-destructive testing. John Wiley & Sons, Inc, ISBN 0-471-18190-0.

Palumbo D., Tamborrino R., Galietti U., Luprano V.A.M. (2016). Ultrasonic analysis and lock-in thermography for debonding evaluation of composite adhesive joints. NDT & E International Volume 78, Pages 1-9.

Tamborrino R., Palumbo D., Galietti U., Aversa P., Chiozzi S., Luprano V.A.M., (2016). Assessment of the effect of defects on mechanical properties of adhesive bonded joints by using non-destructive methods. Composites Part B, 91, 337-345.

Palumbo D., De Finis R., Demelio G.P., Galietti U. (2016). A new rapid thermographic method to assess the fatigue limit in GFRP composites. Composite Part B, 103, 60-67.

Palumbo D., Galietti U. (2017). Thermal Methods for Evaluating Flaws in Composite Materials: A New Approach to Data Analysis. Mechanics of Composite and Multi-functional Materials. Volume 7, Proceedings of the 2016 Annual Conference on Experimental and Applied Mechanics, pp. 267-275, ISBN: 978-3-319-41765-3, DOI: 10.1007/978-3-319-41766-0_32.

Palumbo D., De Finis R., Demelio G.P., Galietti U. (2017). Study of damage evolution in composite materials based on the Thermoelastic Phase Analysis (TPA) method. Composite Part B, 117, 49-60.

Galietti U., Palumbo D., Calia G., Pellegrini M. (2012). Non-destructive evaluation of composite materials with thermal methods. 15th European

Conference on Composite Materials (ECCM 15), Venice (Italy), ISBN 978-88-88785-33-2.
Galietti U., Dimitri R., Palumbo D., Rubino P. (2012). Thermal Analysis and Mechanical Characterization of GFRP Joints. 15th European Conference on Composite Materials (ECCM 15), Venice (Italy), ISBN 978-88-88785-33-2.
Sun J. (2013). Analysis of data processing methods for pulsed thermal imaging characterisation of delaminations. Quantitative InfraRed Thermography Journal 10(1):9-25 .
Balageas D.L. (2012). Defense and illustration of time-resolved pulsed thermography for NDE. Quantitative InfraRed Thermography Journal 9:3-32
Junyan L., Jinlong G., Fei W., Yang W. (2016). Study on probability of detection (POD) determination using lock-in thermography for nondestructive inspection (NDI) of CFRP composite materials. Infrared Physics & Technology Manuscript Draft: INFPHY-D-15-00120
Hidalgo-Gato R., Andrés J. R., López-Higuera J. M., Madruga F. J. (2013). Quantification by Signal to Noise Ratio of Active Infrared Thermography Data Processing Techniques. Optics and Photonics Journal, 2013, 3, 20-26.
Ibarra-Castanedo C., Bendada A. and Maldague X. (2007). Thermographic Image Processing for NDT. IV Conferencia Panamericana de END Buenos Aires.
Ibarra-Castanedo C., Bendada A. and Maldague X. (2005). Image and signal processing techniques in pulsed thermography. GESTS Int'l Trans. Computer Science and Engr., 22(1): 89-100.
Shepard S. M. (2001). Advances in Pulsed Thermography. Proc. SPIE - The International Society for Optical Engineering, Thermosense XXVIII, Orlando, FL, 2001, Eds. A. E. Rozlosnik and R. B. Dinwiddie, 4360:511-515.
Ibarra-Castanedo C. (2005). Quantitative subsurface defect evaluation by pulsed phase thermography: depth retrieval with the phase, Collection Mémories et thèses électroniques.
Maldague X., Couturier J.-P., Marinetti S., Salerno A., Wu D. (1996). Advances in pulsed phase thermography. Quantitative InfraRed Thermography Journal 10.21611/ 1996.062
Rajic N. Principal Component Thermography. (2002) DEFENCE SCIENCE & TECHNOLOGY, Airframes and Engines Division Aeronautical and Maritime Research Laboratory, DSTO-TR-1298.
Rajic N. Principal Component Thermography. DEFENCE SCIENCE & TECHNOLOGY, Airframes and Engines Division Aeronautical and Maritime Research Laboratory, DSTO-TR-1298.
Parvataneni R. (2009) PRINCIPAL COMPONENT THERMOGRAPHY FOR STEADY THERMAL PERTURBATION SCENARIOS. Clemson University, All Theses.Paper 702.
Balageas D.L., Roche J.M., Leroy F.H., Gorbach A.M. (2013). THE THERMOGRAPHIC SIGNAL RECONSTRUCTION METHOD: A POWERFUL TOOL FOR THE ENHANCEMENT OF TRANSIENT THERMOGRAPHIC IMAGES. ICB Seminar 2013 on "Advances of IR-thermal imaging in medicine" Warsaw (Poland).
Benitez H., Ibarra-Castanedo C., Loaiza H., Caicedo E., Bendada A., Maldague X. (2006). Defect Quantification with Thermographic Signal Reconstruction and Artificial Neural Networks. . Quantitative InfraRed Thermography Journal 10.21611/2006.010.
Balageas D. L., Chapuis B., Deban G., and Passilly F. (2010). Improvement of the detection of defects by pulse thermography thanks to the TSR approach in the case of a smart composite repair patch. 10th International Conference on Quantitative InfraRed Thermography.
Palumbo D., Ancona F., Galietti U. (2014). Quantitative damage evaluation of composite materials with microwave thermographic technique: feasibility and new data analysis. Springer Meccanica 50:443–459.
Palumbo D. and Galietti U. (2016). Damage Investigation in Composite Materials by Means of New Thermal Data Processing Procedures. Strain 52(4):276-285
Giorleo G. and Meola C. (2002). Comparison between pulsed and modulated thermography in glass-epoxy laminates. NDT&E International 35, 287-292.
Balageas D.L., Roche J.M. and Leroy H. (2017). Comparative Assessment of Thermal NDT Data Processing Thecniques for Carbon Fiber Reinforced Polymers, Materials Evaluation 75(8):1019-1031.